Spring 5-12-2017

SYNTHESIS AND CHARACTERIZATION OF MOLYBDENUM SULFIDE AND FOR HYDROGEN EVOLUTION REACTION AND SUPERCAPACITOR APPLICATIONS

Zhuo Wang
Pittsburg State University, zwang@gus.pittstate.edu

SYNTHESIS AND CHARACTERIZATION OF MOLYBDENUM DISULFIDE FOR HYDROGEN
EVOLUTION REACTION AND SUPERCAPACITOR APPLICATIONS

A Thesis Submitted to the Graduate School
in Partial Fulfillment of the Requirements
for the Degree of
Master of Science

Zhuo Wang

Pittsburg State University

Pittsburg, Kansas

May, 2017

SYNTHESIS AND CHARACTERIZATION OF MOLYBDENUM DISULFIDE FOR HYDROGEN
EVOLUTION REACTION AND SUPERCAPACITOR APPLICATIONS

Zhuo Wang

APPROVED:

Thesis Advisor   _____
                     Dr. Ram Gupta, Department of Chemistry

Committee Member   _____
                     Dr. Pawan Kahol, Department of Physics

Committee Member   _____
                     Dr. Khamis Siam, Department of Chemistry

Committee Member   _____
                     Dr. Charles Neef, Department of Chemistry

ACKNOWLEDGEMENTS

SYNTHESIS AND CHARACTERIZATION OF MOLYBDENUM DISULFIDE FOR HYDROGEN
EVOLUTION REACTION AND SUPERCAPACITOR APPLICATIONS

An Abstract of the Thesis By
Zhuo Wang

To meet the constant rising requirement of energy, it is a perfect time to develop a low cost and efficient material for clean energy production and storage. Hydrogen generation by water splitting is one of the cleanest ways to produce green and cheaper energy. Hydrogen evolution reaction (HER) is one of the key steps in water splitting process. Ideally, the thermodynamic potential for HER should be at 0 V (vs. SHE). However, without an efficient catalyst, this reaction occurs at higher potential, called overpotential. A good HER catalyst is needed to lower the overpotential and improve the energy efficiency of this process. Presently, platinum is the most effective and durable catalyst for HER, but its wide spread use is precluded due to its high cost. Therefore, it is essential to develop low-cost and earth-abundant materials to replace precious-platinum based catalysts which could be also used for energy storage applications. In this work, a facile and scalable one-pot method has been used to synthesize carbon coated molybdenum disulfide (MoS_2). The carbon coated MoS_2 is advantageous as this increases the electrical/ionic conductivity of MoS_2. The structural characterizations of MoS_2 and carbon coated MoS_2 was performed using x-ray diffraction and scanning electron microscopy. Electrochemical behavior of hydrogen evolution reaction was studied in potential range of 0 to -0.7 V. Our results suggest that carbon coated MoS_2 needed lower overpotential compared to uncoated MoS_2. The lowest overpotential for carbon-coating MoS_2 material was observed to be 133 mV, which was much lower than the uncoated MoS_2 sample (180 mV). Further electrochemical properties of the synthesized MoS_2 samples were studied using cyclic voltammetry and galvanostatic charge-discharge methods. Optimized carbon coated

MoS$_2$ showed a specific capacitance of 299 F/g in 3M KOH at scan rate of 1 mV/s. Our studies opened up a new pathway to synthesize cost effective MoS$_2$ which could be used for hydrogen evolution reaction and energy storage applications.

TABLE OF CONTENTS

LIST OF TABLES

LIST OF FIGURES

CHAPTER I

INTRODUCTION

This master's thesis has been organized into four chapters. Chapter I describes a brief introduction of various kinds of materials for energy generation and storage. It also describes the flaws and advantages of past materials used for energy applications. Chapter II provides the experimental details about the synthesis of molybdenum disulfide. It presents a comprehensive theoretical background of different techniques used for characterizations of molybdenum disulfide. Subsequently, chapter III is dedicated to the results and discussion of the various experimental techniques used in this research. Finally, the conclusion of this research work is discussed in chapter IV.

1.1 Importance of energy

As energy continues to be in demand due to increasing and ongoing usage of electronic appliances, there is an urgent need to develop efficient but low-cost energy conversion and storage devices. There are several ways to get energy apart from conventional sources, such as coal, gas, and petroleum. Some of the typical non-conventional (green) energy sources are solar light, hydro-power, and wind energy. In this modern society, they play critical roles in satisfying the energy need in different areas around the world. However, their supply lacks the demand

and their non-consistent mode of energy generation (wind) and lacking efficiency (solar energy) limits their level of effectiveness as energy generation devices.

Devices based on conversion of solar light into electricity are the most common for practical applications. These devices are also known as solar cells or photovoltaic devices. The research on solar cells is divided into three generations. The first generation is the classic solar cell where silicon was used as main material for light to energy conversion. The silicon wafer was used to fabricate such devices. The second generation of solar cells was based on non-silicon thin-film such as cadmium telluride. The third generation utilizes various materials such as solar dyes, conducting polymers, flexible electrodes. However, solar cells can only generate energy during the day time (while in sunlight) and engender the need for other resources to support energy need at night.

Wind energy is another source to generate energy. Wind energy is also considered as one of the greenest ways to generate clean energy. However, due to the major dependence over high thrust wind, wind energy lacks a consistent supply over time. Hydro-energy is the other main type of non-conventional energy source by which energy can be generated. There are many different types of hydro-energy, such as small hydro, micro hydro, conventional hydroelectric, run-of-the-river hydroelectricity, and pumped storage hydroelectricity. Of all types, hydropower is the most efficient and consistent source of energy production. However, there are limited water sites that could support this kind of energy generation. From all the above observations, there seems to be an essential need for a consistent and efficient green energy production and storage.

1.2 Fuel cells and classifications

A fuel cell is a device that converts chemical energy from a fuel into electricity energy. Ethanol, methanol, and hydrogen fuel cells are some of the emerging devices. Of these, hydrogen is among the most favored source because hydrogen fuel cells produce non-harmful water as a byproduct. Fuel cells can produce electricity continuously for as long as the required chemicals are supplied.

The first fuel cells were invented by William Robert Grove, a British scientist, in 1838 [1]. The first commercial application for the fuel cell came more than a century later in the space projects of NASA to generate a constant power supplement for satellites and space capsules [2]. Since then, fuel cells have been commercially used in many other fields. Fuel cells are used as primary and backup power sources for industrial and residential buildings and in sealed, narrow, or inaccessible areas. They are also used to power fuel-cell vehicles, including automobiles, buses, boats, motorcycles, forklifts, and submarines.

Proton exchange membrane fuel cells (PEMFCs) are a type of fuel cells that were developed for applications of vehicles' motivation, stationary settings, and portable devices. The most typical features include a special polymer membrane, which is the core component [3]. They are built out of membrane electrode assemblies (MEA), which are composed of two electrodes, electrolyte, catalyst, and diffusion layers. A mixture of carbon, catalyst, and electrode is sprayed or painted on the solid electrolyte and two carbon papers were attached on either side of the electrolyte as electrodes. The central part of the cell is the triple-phase interface where the reactants, electrolyte, and catalyst contact each other. This is the part where reactions actually occur. This kind of fuel cell is commercially used because of its low temperature application and portability.

Solid oxide fuel cells (SOFCs) are another type of fuel cells which are operated at high temperatures (500-1000 °C). SOFCs convert electricity directly from oxidizing a fuel. The typical feature of SOFCs is the special electrolyte which is a solid oxide or ceramic. The most prominent advantage of these fuel cells is that the expensive catalyst such as platinum is not required. However, high operating temperature, which results in longer start-up times, chemical, and mechanical compatibility is the significant drawbacks of such fuel cells.

Molten-carbonate fuel cells (MCFCs) are a type of fuel cells whose mechanism is very similar to that of SOFCs but use an electrolyte composed of a molten carbonate salt mixture adsorbed in a porous ceramic matrix of beta-alumina solid-electrolyte (BASE). The operating temperature of such fuel cell is high (about 650 °C to keep carbonate salt in its molten phase). They have advantages similar to SOFCs, but their corrosive nature due to molten carbonate salt is high, which limits their cell life.

Alkaline fuel cells (AFCs), also known as the Bacon fuel cells after its British inventor, Francis Thomas Bacon, is one of the most developed fuel cell technologies [4]. NASA has applied these technologies in space shuttle and Apollo-series missions since 1960s [1]. In these fuel cells, hydrogen and oxygen are consumed in potassium hydroxide solution electrolyte to produce water, heat, and electric power. The potential conversion efficiency could be as high as 70%. However, the unique disadvantage of AFCs is that the carbon dioxide impurity in gas reacts with the potassium hydroxide electrolyte into potassium carbonate and will fill into the pores of the carbon electrode's which decreases the efficiency of the fuel cell. A high purity gas is required to avoid this.

Out of all different types of fuel cells, hydrogen fuel cell is one of the most exciting and widely researched ways for energy generation. Splitting of water enables an easy source of highly pure hydrogen, which can be used as a fuel. Apart from being a light molecule, it has high

calorific value compared to other fuels. Moreover, it generates harmless byproduct after

burning. Ease in availability of water has enabled its high productive capability.

1.3 Hydrogen evolution reaction (HER)

Hydrogen evolution reaction is defined as "production of hydrogen through water

electrolysis". It is commonly used to evaluate the anode catalyst's performance. In the context

of fuel cells, it is used to refer to half reaction of water electrolysis as below:

$$2H^+ + 2e^- \rightarrow H_2\,(g) \,\ldots\ldots\ldots\ldots\ldots\ldots\ldots\ldots\ldots.(1)$$
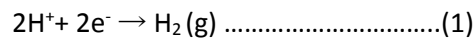
In this procedure there are two steps, as shown in Figure 1.1.
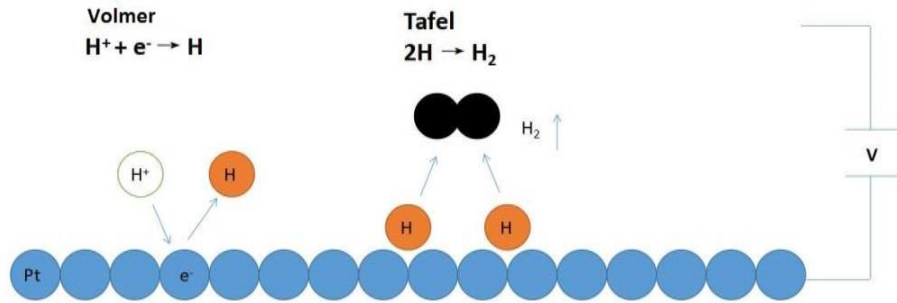
Figure 1.1: Volmer and Tafel steps

In Figure 1.1, the Volmer step (1st step) and Tafel step (2nd step) happen on an anode

which contains a catalyst such as platinum on its surface. During these two steps, a certain

amount of potential will be lost due to reaction activation, called overpotential. The

overpotential depends on the properties of the catalyst. Basically, lower overpotential means

5

better water splitting process. Linear scanning voltammetry (LSV) test and corresponding Tafel slope provide information about the performance of the catalysts.

1.4 Main stream development of fuel cell technologies

The main components of fuel cells are anode, cathode, and electrolyte (Fig 1.2). Anode and cathode are separated using proton transporting layer which allow positively-charged hydrogen ions to move between the two sides of the fuel cell. Electrical current is generated by this positive ion flow. The anode and cathode contain catalysts, which cause the fuel to undergo oxidation reactions that generate positively charged hydrogen ions and electrons. The hydrogen ions are drawn through the electrolyte after the reaction ($2H_2 + 2O^{2-} \rightarrow 2H_2O + 4e^-$). At the same time, electrons are drawn from the anode to the cathode ($O_2 + 4e^- \rightarrow 2O^{2-}$) through an external circuit, producing direct current electricity. At the cathode, hydrogen ions, electrons, and oxygen react to form water ($2H_2 + O_2 \rightarrow 2H_2O$). Various kinds of electrolytes are being used for fuel cells. Fuel cells are classified by the types of electrolyte used and the difference in launch time ranging from 1 second for proton exchange membrane fuel cells to 10 minutes for solid oxide fuel cells [5]. Single cell generates relatively low electrical potential (about 0.7 V), so these cells are always stacked, or placed in series, to create sufficient voltage to meet an application's requirements. In addition to produced fuel, they also produce water, heat and other byproducts, depending on the distinct kinds of fuel sources. The energy efficiency of a fuel cell is generally between 40 - 60% which could be improved up to 85%, if generated heat is recycled.
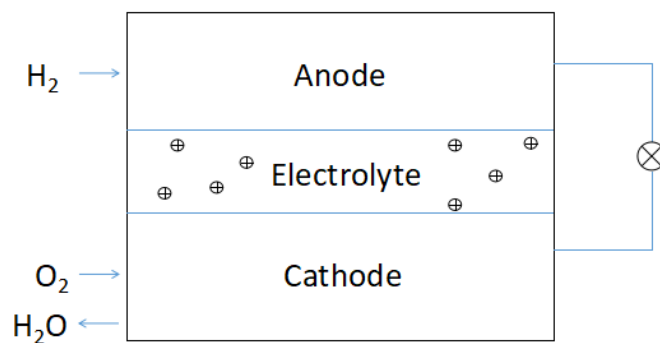
Figure 1.2: A block diagram of a fuel cell

The development of new catalyst for fuel cell is a key factor to improve its performance and reduce cost. Platinum deposited film was used as the catalyst material on the anode of fuel cell in 1958 by Leonard Niedrach, a scientist of General Electric Company (GE) [6]. Platinum is an excellent catalyst for hydrogen evolution reaction, but is very expensive and requires in very pure form (to prevent the catalyst poisoning by impurities). Platinum is so sensitive that trace of impurities such as carbon monoxide will deactivate it [7].

For commercialization of fuel cells, it is essential to have an effective and low cost catalyst that would be practical enough to replace platinum. Recently, transition metals such as molybdenum, cobalt, iron, and zinc based compounds have attracted considerable research interest for their applications as catalysts in fuel cells and electrode materials for energy storage. These transition metals have relatively loose electron cloud structures which lead to easy-accessing and disengagement with reacting chemicals. In addition, they are relatively cheaper in price and easily available.

Morphology and active surface area are other factors which determine the quality catalysts. Recently, most of the research works are focusing on increasing surface area of catalysts to improve their efficiency [3]. Mainstream technology in this field is using carbon

nanotube or graphene nanosheet as the support base of these transition metal compounds to increase the surface area [8,9,10]. Although this method is very effective, the cost of carbon nanotubes and graphene are high.

1.5 Supercapacitor

Batteries are widely used energy storage devices which convert chemical energy into electrical energy. They could be primary or rechargeable in nature. The crucial issues faced by current batteries are the slow process kinetics and low rate of ionic diffusion/migration, resulting in limited practical energy output and battery performance. In contrast, a capacitor works in a different way. A capacitor stores energy electrostatically in form of an electric field. The most common capacitors consist of conducting plates which are separated by non-conducting layer. These conducting plates are filled with dielectric materials. The potential difference (V) across the plates generates an electrical field in the dielectric material causing generation of positive charge (+Q) at one plate and negative charge (-Q) at other plate. The capacitance (C) of the device is equal to Q/V. Capacitors are called supercapacitor if their charge storage capacity is much higher than conventional double layer capacitor. Supercapacitors are also called ultra-capacitors. They deliver high power and energy density, while batteries offer only high energy density. In addition, supercapacitors demonstrate excellent cyclic stability and long life.

The charge storage mechanism of a capacitor can be divided into two categories: (i) electrical double-layer capacitors (EDLC) in which the capacitance arises from the charge separation at the electrode/electrolyte interface; and (ii) redox electrochemical capacitors (pseudocapacitors) in which the capacitance arises from Faradic reactions occurring at the electrode interface.

As in electrochemical double layer capacitors, the capacitance increases from the charge separation at the electrode/electrolyte interface, an electrode with larger surface area could store a larger amount of charge. The commonly-used materials for electrochemical double layer capacitors are carbon based materials. Several types of carbon such as carbon black, graphite, carbon aerogel, carbon fibers and activated carbon are particularly useful for making electrodes for such capacitor [11, 12, 13]. Different types of electrolytes can be also used such as aqueous, non-aqueous, organic and inorganic. Aqueous electrolytes such as sulfuric acid (H_2SO_4) and potassium hydroxide (KOH) are widely used electrolytes. The disadvantage of aqueous electrolytes is their potential limit. The potential limit for aqueous electrolytes is 1.23 V. However, higher potential limit of about 2.5 V can be achieved by using organic electrolytes.

Pseudocapacitance arises at the electrode surfaces where the charges are Faradically stored. The most commonly used materials for pseudocapacitors are metal oxides, metal sulfides and conducting polymers [14, 15, 16]. Among the metal oxides, various transition-metal oxides, such as RuO_2, Co_3O_4, NiO, Fe_2O_3, Fe_3O_4 and MnO_2 are being used. Pseudocapacitors provide high energy density but low power density. Hybrid capacitors are the capacitors which utilize properties of both electrochemical double layers and pseudocapacitors. Hybrid capacitors are better than electrical double-layer capacitors and pseudocapacitors due to combined properties of both double layer and Faradic reactions at electrode providing high power and energy density. Table 1.1 describes the advantages and disadvantages of a supercapacitor.

Table 1.1: Advantages and disadvantages of supercapacitors

Advantages	Disadvantages
No chemical reaction	Energy density is low
Simple charging requires	Need cell balancing
Charges faster than batteries	Self-discharge is high
Longer operation life (more than 10 years)	
Controlled charging behavior (no overcharge)	
Provides high power density	

1.6 Project rationale

In this study, a facile method was used to synthesize carbon@MoS$_2$ as a catalyst for hydrogen evolution reaction in water splitting process and as an electrode material for energy storage application.

MoS$_2$ as a typical layered transition metal sulfide has an analogous structure to graphite and a significantly larger interlayer distance of *ca.* 0.6 nm,[17] which allows a fast diffusion path for movement of ions and can be used as a catalyst and an active material for energy storage applications. However, there are some inherent problems with MoS$_2$ which hamper its application for energy such as:

1. Short cycling life due to the collapsing of functional structure which caused by the large volume charge during testing cycles [18],

2. Low coulombic efficiency due to the formation of a solid electrolyte interface film from degradation of electrolyte [19],

3. Low utilization and limited rate capacity caused by the poor electronic conductivity of MoS$_2$

In order to solve these problems, several technological potential solutions have been attempted.[20,21] Improvements can be achieved through compositing MoS_2 with the conductive carbon-based materials, such as amorphous carbon [22,23], carbon nanotubes [24,25], ordered mesoporous carbons [26], or graphene [27,28]. The conductive carbon structure provides the elastic support and generates essential electrical contact for MoS_2 [29]. Meanwhile, the carbon phase acts as a shield layer and then defense the degradation of the electrode [30]. As a result, the effective utilization of MoS_2 and the life time can be improved. Another effective method to improve the catalytic properties is making MoS_2 materials on the nanometer scale such as nanospheres [31], nanorods [32], nanotubes [33], and nanosheets [34]. Furthermore, constructing hierarchical three-dimensional architectures of MoS_2 could provide high stability and large surface area [35]. Such architectures can assist in enhancing the feature of both nano-materials and micro-materials, and provide sufficient hollowed spaces between the nanosheets which effectively ease the external mechanical stress and charge volume striking during the charge-discharge cycles [36].

CHAPTER II

EXPERIMENTAL DETAILS

2.1 Material and synthesis

2.1.1. Preparation of carbon@MoS₂ (C@MoS₂) core-shell microspheres

Carbon@MoS$_2$ (C@MoS$_2$) core-shell microspheres were synthesized via a facile one-pot hydrothermal method and subsequent heat-treatment. In a typical synthetic procedure, resorcinol (0.44 g, 4 mmol) and formaldehyde (0.645 g, 37 wt%, 8 mmol) were dissolved in distilled water (15 ml) and then stirred at 40 °C for 1 h (named RF solution). Subsequently, melamine (0.505 g, 4 mmol) and formaldehyde (0.97 g, 37 wt%, 12 mmol) were dissolved in distilled water (15 ml) and heated to 80 °C with consecutive agitation until the solution became clear (called MF solution). MF solution was cooled down to 40 °C and then added into the RF solution with continuous stirring for 30 min, to form MRF solution. Na$_2$MoO$_4$ (1.20 g) and NH$_2$CSNH$_2$ (2.40 g) were dissolved in MRF solution, and was then transferred to a 45 ml Teflon lined autoclave (Parr) and heated at 180 °C for 24 h. The precipitate was collected by filtration, washed with distilled water, and dried at 100 °C, to form uncarbonized MRF@MoS$_2$ core-shell microspheres. The carbon-coated C@MoS$_2$ microspheres were synthesized by carbon coating the above uncarbonized MRF@MoS$_2$ core-shell microspheres by adding glucose through in-situ hydrothermal polymerization and carbonization. Typically, MRF@MoS$_2$ core-shell microspheres (2.25 g) were re-dispersed in distilled water (31.5 ml) containing glucose (0.45 g) and transferred

into a 45 ml Teflon lined autoclave. The autoclave was heated at 180 °C for 12 h. The resulting carbon-coated C@MoS$_2$ microspheres were obtained by filtration, drying at 100 °C, and carbonization at 800 °C (10 °C/min) for 3 h in N$_2$ flow. Various samples having different amount of glucose were synthesized using the above method (Table 2.1). Figure 2.1 shows the schematic of synthesis of hierarchical C@MoS$_2$ core-shell microspheres.

Table 2.1: Sample name and quantity of glucose added during synthesis of carbon-coated C@MoS$_2$ samples

Sample name	Glucose added (g)
MS-1	0
MS-2	0.2
MS-3	0.4
MS-4	0.6
MS-5	1.5
MS-6	2.5
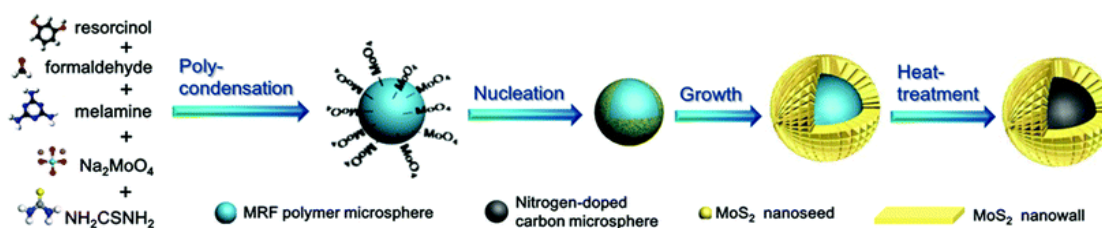
Figure 2.1 Schematic representation of the formation process of the hierarchical C@MoS$_2$ core-shell microspheres. (Adopted [17] with permission from Royal Society of chemistry, Nanoscale 7, 2015, 13043)

2.2 Structural characterization

The synthesized materials were structurally characterized using many techniques such as X-ray diffraction (XRD), scanning electron microscopy (SEM), energy-dispersive X-ray spectroscopy (EDX), Raman spectrum and thermogravimetric analysis (TGA).

2.2.1 X-ray diffraction

X-ray diffraction technique was used to study crystallinity, phase purity, and interlayer distance of the synthesized MoS_2 samples. The principle of XRD measurement is based on measuring the x-ray intensity which was diffracted through a material into many specific directions (Fig 2.2). XRD measurements were performed using Shimadzu x-ray diffractometer with $CuK_{\alpha 1}$ (λ=1.5406 Å) as the radiation source. 0.2 mm slits were used for the source and detector sides. XRD was operated at a voltage of 40 kV and a current of 30 mA.
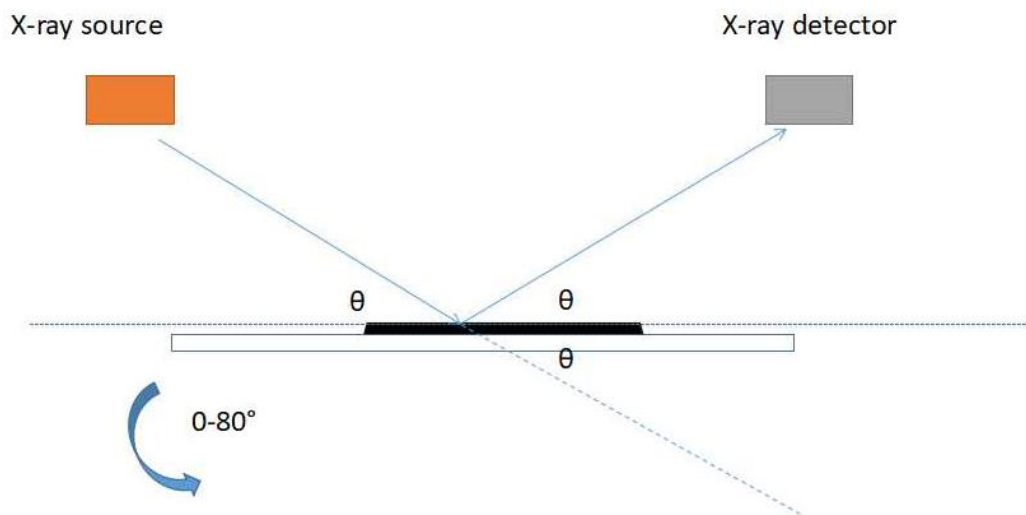
Figure 2.2: Principle of XRD

2.2.2 Scanning electron microscopy and energy-dispersive X-ray spectroscopy

The morphologies of the synthesized MoS_2 materials were examined using scanning electron microscopy. The SEM is a valuable instrument in the development of scientific theories and has contributed greatly towards the advancement of materials science and other areas. The principle of SEM is based on analyzing the reflected signals which are caused from interaction of the secondary electron beam with the atoms on the surface of sample in different microcosmic depths. By the feedback analysis, analyzer instrument can present the microcosmic image of the surface of sample. JEOL 7000 FE-SEM was used for all the measurements.

Energy-dispersive X-ray spectroscopy was used for elemental-analysis of samples. The mechanism of this method is based on the specific peak which cause by each element's unique electromagnetic emission spectrum. To stimulate the emission of characteristic x-rays from a sample, a high-energy charged particle beam was focused into the sample. The charged particles of the beam excited some lower-energy shell electrons which caused creation of "electron holes". Electrons from higher-energy shells filled these holes and during this process, they released energy in form of X-ray. Mechanism of EDS is given in Figure 2.3.
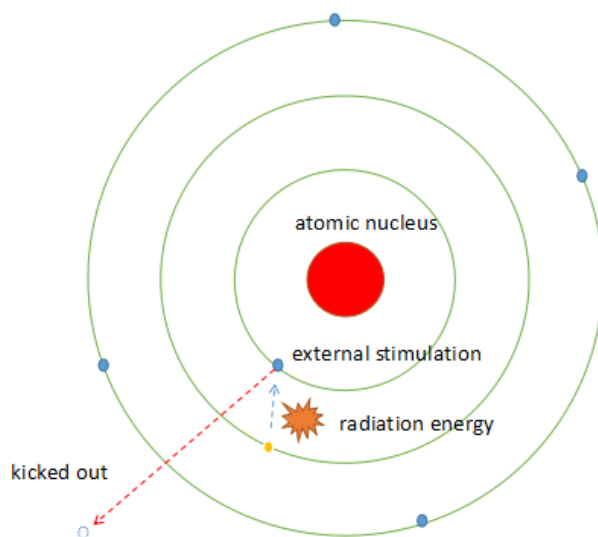
Figure 2.3 Mechanism of EDX

2.2.3 Raman spectroscopy

Raman spectroscopy is commonly applied in chemical characterization of a sample to provide fingerprints of molecules. It relies on Raman scattering of monochromatic light which illuminates the sample in the visible, near infrared or near ultraviolet range. In our experiments, Raman spectroscopy was used to confirm the formation of MoS_2 and to analyze the carbon coating on MoS_2. Raman spectroscopy (Model Innova 70, Coherent) was performed using an argon ion laser at a wavelength of 514.5 nm as the excitation source.

2.2.4 Thermogravimetric analysis

The thermal stability of the synthesized materials was studied using thermogravimetric analysis. In TGA, samples were heating from room temperature to 700 °C at a rate of 10 °C/min in air flow of 40 ml/min and change in weight was recorded using TA 2980 instrument. By analyzing the data, the percentage of carbon in the synthesized carbon coated MoS_2 can be determined.

2.3 Electrochemical characterization

The synthesized materials were electrochemically characterized using linear scan voltammetry (LSV), cyclic voltammetry (CV), galvanostatic charge-discharge (GCD), and electrochemical impedance spectroscopy (EIS).

2.3.1 Hydrogen evolution reaction

Hydrogen is a future resource for energy and it can be generated via water splitting. A good catalyst for electrochemical hydrogen evolution reaction through water splitting should

reduce the overpotential. Overpotential is defined as the potential difference between thermodynamically determined potential and potential at which the redox event is experimentally observed [37]. Linear scan voltammetry was used to determine the overpotential of the synthesized materials and to check their suitability as catalysts for HER application. In LSV, current at a working electrode was measured while the potential between the working electrode and a reference electrode was scanned linearly in specific voltage range (Figure 2.4).
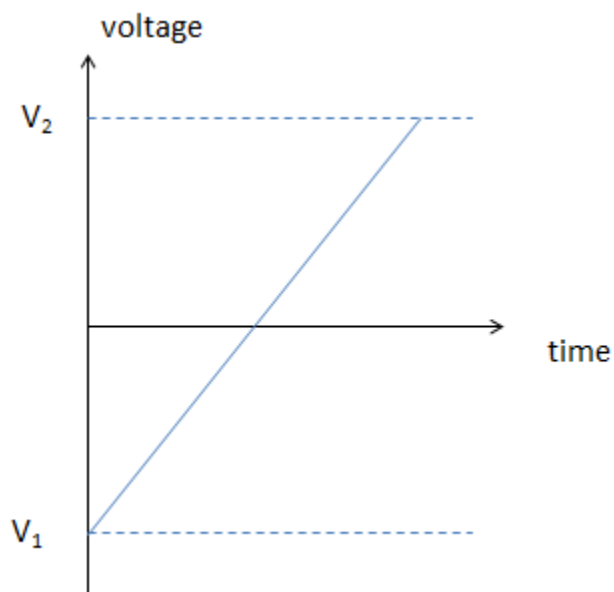
Figure 2.4 Variation rate of voltage in LSV process

In LSV test of MoS_2 materials, two parameters were emphasized: (1) the maximum current which test curves can reach (Fig 2.5), and (2) Tafel slope of each sample (Fig 2.6). As for Tafel slope, it is an experimental-measuring parameter which indicates the slope rate of the curve on overpotential. Based on the chart below, I is the current produced by catalyst material in HER test under specific voltage.
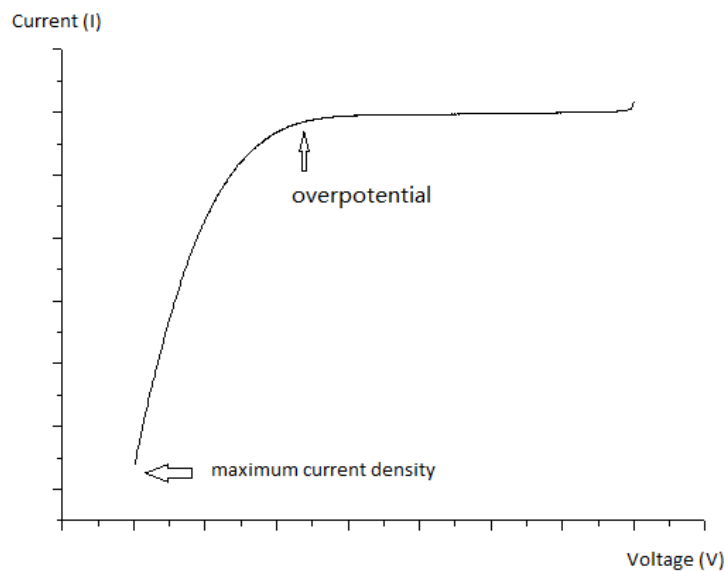
Figure 2.5 Typical HER plotting
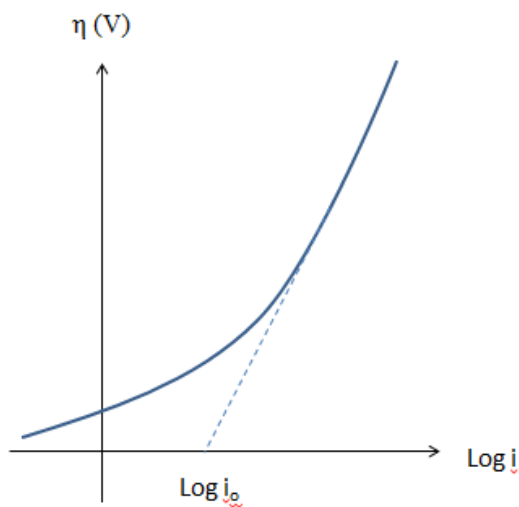
Figure 2.6 Tafel plot for an anodic process

where η is the overpotential, i is current density (A/m^2) and i$_0$ is exchange current density (A/m^2)

A Versastat 4-500 electrochemical workstation (Princeton Applied Research, USA) was used for the electrochemical measurements. A graphite and Ag/AgCl electrode were used as a counter electrode and a reference electrode, respectively. Working electrode was prepared by

dropping 10 µl inks which was made using sample (2.5 mg), distilled water (0.125 ml), ethanol 0.125 ml, and Nafion (6.25 µl) on glass-carbon electrode. 1M H_2SO_4 was used as an electrolyte.

2.3.2 Electrochemical impedance spectroscopy

Electrochemical impedance spectroscopy was further used to characterize the synthesized materials. EIS measurements were performed at various potentials in frequency range of 0.05 Hz to 10 kHz.

2.3.3 Cyclic voltammetry for fuel cell application

In fuel cell part of the research, CV test was used to estimate the electrochemical active surface area of each sample. The CV test was performed in non-Faradic region to estimate real electrochemical active surface area. Figure 2.7 shows the principle of CV test, where samples are scanned between two potentials with a certain scan rate.
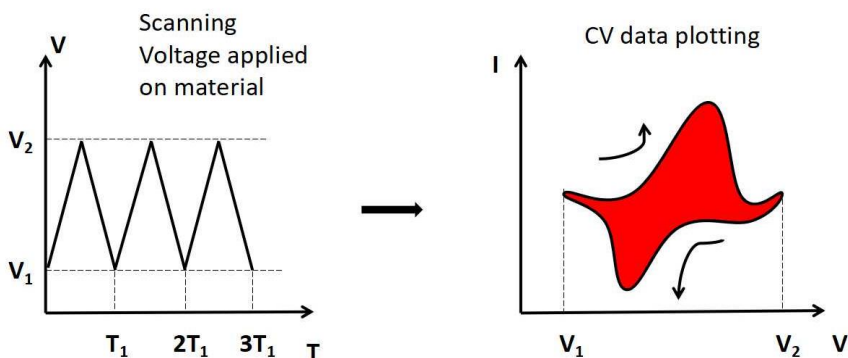
Figure 2.7 Principle of CV test

2.3.4 Cyclic voltammetry for supercapacitors

Working electrodes for electrochemical measurements were prepared by coating viscous slurry of 80% (w/w) C@MoS_2, 10% (w/w) of acetylene black, and 10% (w/w) of polyvinylidene difluoride (PVDF) in N-methyl pyrrolidinone (NMP) onto nickel foam. The coated

nickel foam was dried under vacuum at 60 °C for 10 h. Standard three electrode measurement system was used. MoS_2 coated on nickel foam, platinum wire and saturated calomel electrode was used as working, counter and reference electrodes, respectively. All the measurements were performed in 3M KOH aqueous solution. The charge storage capacity of the electrode was determined using cyclic voltammetry and galvanostatic charge-discharge method. Gravimetric specific capacitance was calculated using the expression:

$$C_g = \frac{Q}{\Delta V \times (\frac{\partial v}{\partial t}) \times m} \quad \text{................2.1}$$

where, C_g is the gravimetric capacitance (F/g), Q is the area under the CV curve (C), $\partial v/\partial t$ is the scan rate (V/s), ΔV is the potential range, and m is the mass of the sample (g).

2.3.5 Galvanostatic charge-discharge method for supercapacitors

In galvanostatic charge-discharge measurements, the working electrode was charged from 0 to 0.56 V using various current densities (0.25A/g, 0.5 A/g, 0.75 A/g, 1A/g, 1.5A/g, 2A/g, 3A/g, 4A/g and 5A/g). The gravimetric specific capacitance from GCD measurements was calculated by the equation given below:

$$C_g = \frac{I \times \Delta t}{\Delta V \times m} \quad \text{................2.2}$$

where C_g is the gravimetric capacitance (F/g), I is the discharge current (A), Δt is the discharging time (s), ΔV is the potential range, and m is the mass of the synthesized material (g).

CHAPTER III

RESULTS AND DISCUSSION

3.1 X-ray diffraction

X-ray diffraction patterns of all the samples were recorded in two theta range of 10 – 80° to determine the crystal structure and phase purity of the synthesized samples. XRD patterns of all the samples are displayed in Figure 3.1. The XRD peaks corresponded to (002), (101), (103), (110), (200) and (116) planes can be indexed to the standard diffraction patterns of crystalline and hexagonal MoS_2 (JCPDS card No.37-1492) [38]. It was observed that XRD peaks related to the (002) and (103) planes became broader and less intense with increase in the amount of glucose during hydrothermal synthesis. This suggests that higher amount of glucose during synthesis reduces the crystallinity of MoS_2 due to increased amount of disordered carbon on MoS_2.
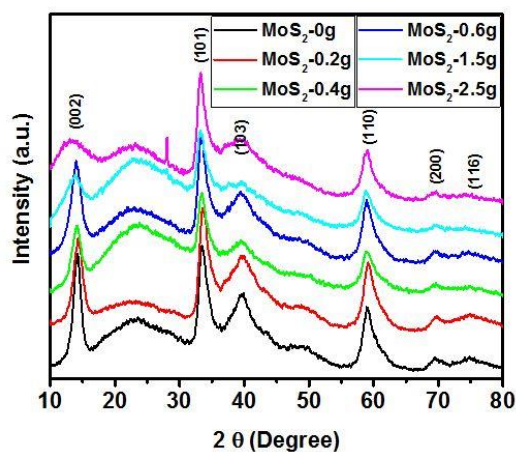
Figure 3.1 The XRD patterns of the carbon coated and uncoated MoS_2

3.2 Energy-dispersive x-ray spectroscopy

Figure 3.2 illustrates the EDX spectrum of MoS_2 with 0.45 g of glucose. As seen in the spectrum, the synthesized compound was entirely consisted of Mo and S and no other foreign elements were observed. The calculated atomic ratio of Mo and S are given in Table 3.1. The elemental ratio of Mo/S was around 1:2, which confirmed the formation was MoS_2. EDX results are in good agreement with the XRD analysis.
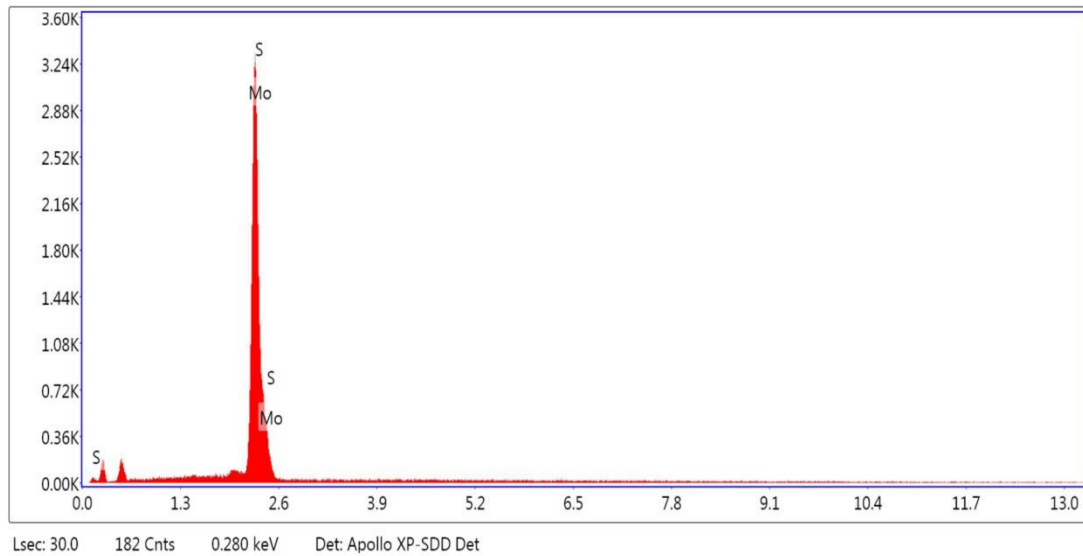
Figure 3.2: EDX spectrum of MoS_2 with 0.45 g of glucose

Table 3.1: Composition analysis of EDX

Element	Weight %	Atomic %	Error %
Mo	64.3	37.6	3.4
S	35.7	62.4	3.3

3.3 Scanning electron microscope

Microstructure and morphology of hydrothermally synthesized carbon coated MoS_2 are shown in Figure 3.3. According to images in Fig. 3.3A-C, synthesized MoS_2 consisted of well-

developed microspheres, clustered together to form an aggregate microstructure. The average diameter of microspheres was around 2 μm. Further magnification into theses microspheres (Figure 3.3D) showed that microspheres were constructed by combining large amount of ultrathin nanowalls which had a thickness of about 25 nm. Nanowalls created a rough surface on the microspheres to increase active surface area of MoS_2. The larger surface area is beneficial to maximize the electrochemical performance of elcetroctalysts and electrode materials.
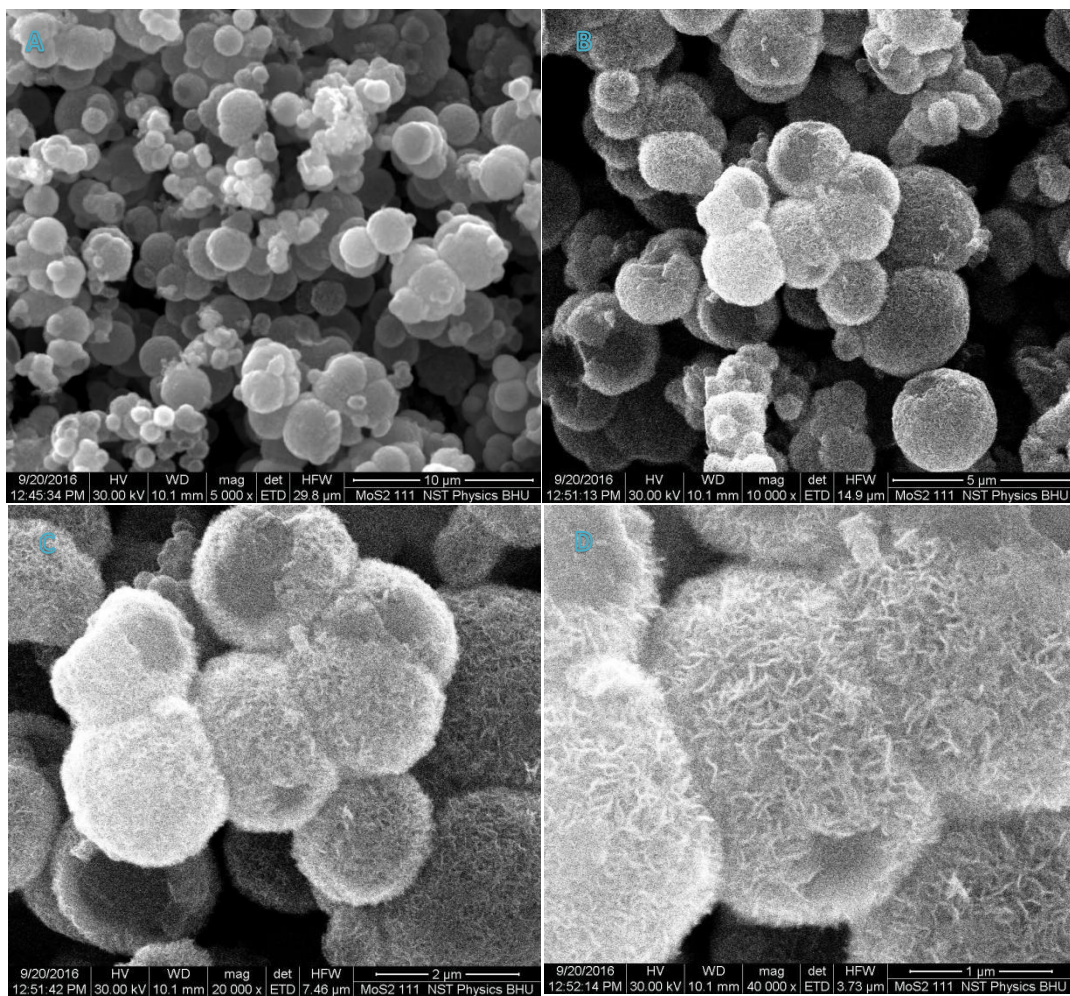
Figure 3.3: SEM images of MoS_2 with 0.45 g of glucose in (A) 10 μm, (B) 5 μm, (C) 2 μm, and (D) 1 μm scale.

3.4 Raman spectra

Raman spectra of the synthesized MoS_2 are shown in Figure 3.4-3.7. As seen in the Raman spectra, peak positions of all the samples were almost similar. Figure 3.8 shows the Raman spectrum of MoS_2 synthesized using 0.2 g of glucose in the range of 200-500 cm^{-1}, highlighting two major characteristic peaks of MoS_2. The peaks at 375 and 415 cm^{-1} correspond to the in-plane E^1_{2g} and out of plane A^1_g modes of hexagonal MoS_2.[39] Relative intensities of between A^1_g and E^1_{2g} mode provided the details about termination structure of crystal MoS_2. Higher intensity of A^1_g mode compare to the E^1_{2g} mode suggested creation of edge terminated MoS_2 crystal structure.[32]
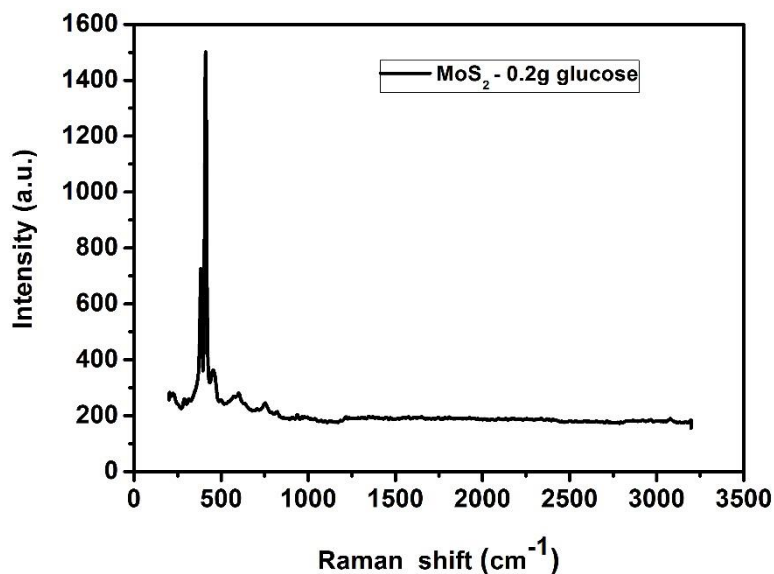
Figure 3.4: Raman spectrum of MoS_2 synthesized using 0.2 g of glucose
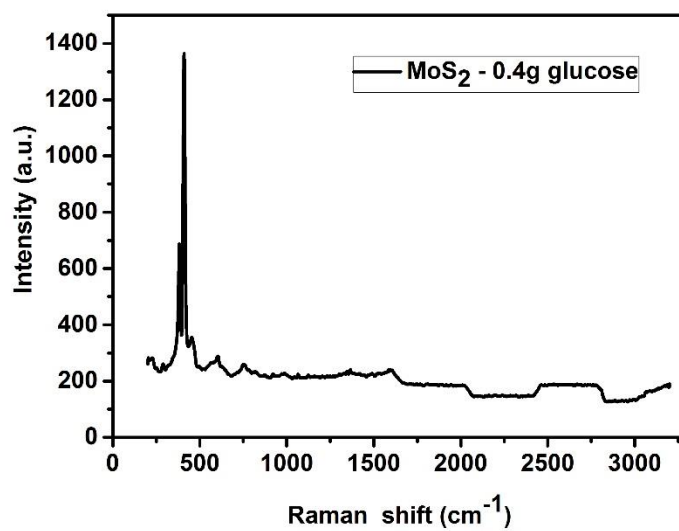
Figure 3.5: Raman spectrum of MoS₂ synthesized using 0.4 g of glucose
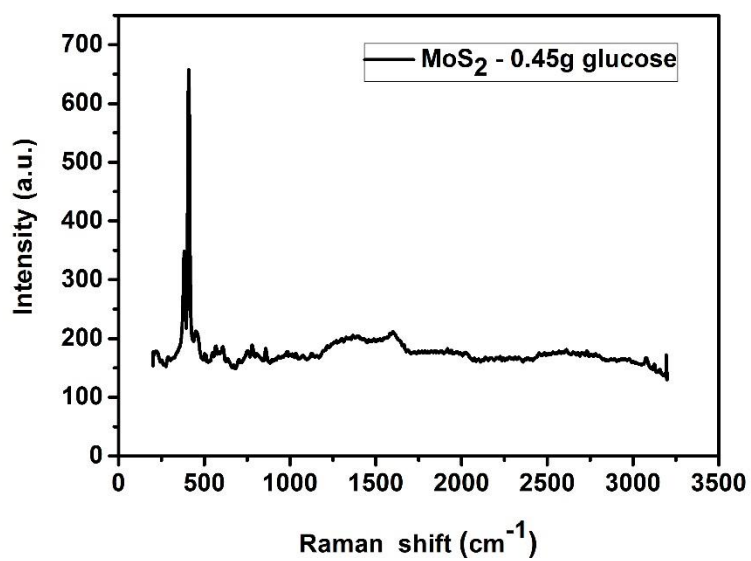
Figure 3.6: Raman spectrum of MoS₂ synthesized using 0.45 g of glucose
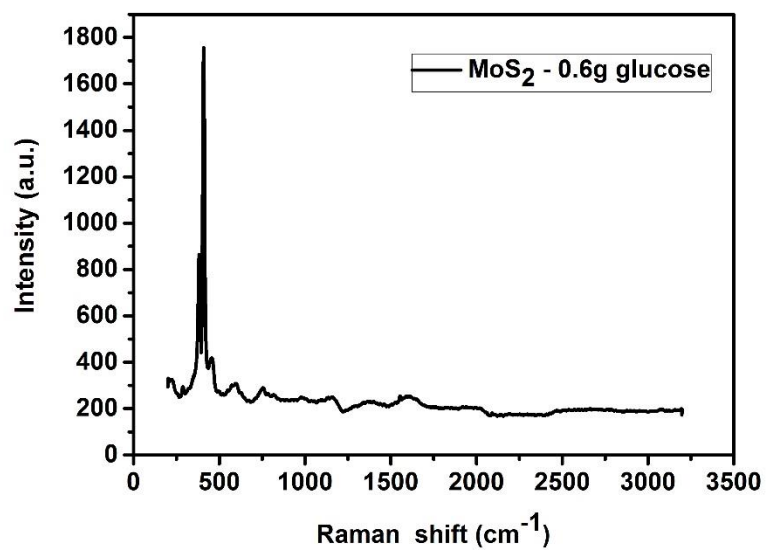
Figure 3.7: Raman spectrum of MoS₂ synthesized using 0.6 g of glucose
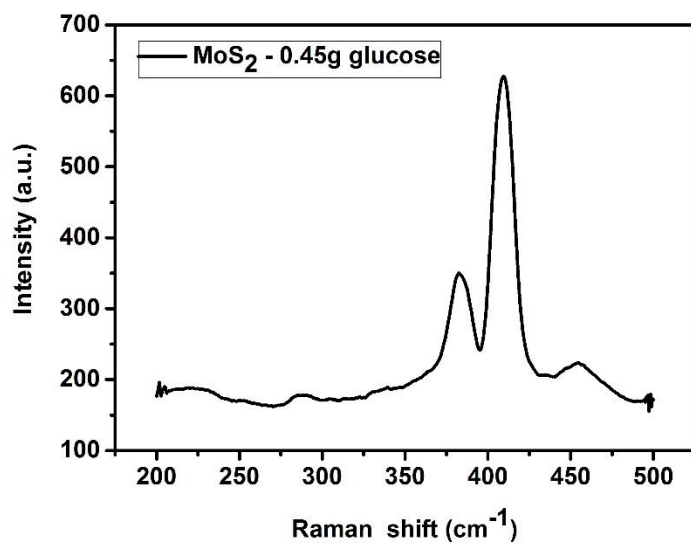
Figure 3.8: Raman spectrum of MoS₂ synthesized using 0.45 g of glucose

3.5 Thermogravimetric analysis

The carbon content in each sample was calculated using TGA residue method and is shown in Table 3.2. The results of thermogravimetric analysis showed that different amount of glucose used during synthesis of MoS$_2$ created carbon coating on MoS$_2$ with varying amount of carbon content. As seen in the TGA curves, all the synthesized MoS$_2$ were thermally stable till 380 °C. The residual amount at higher temperatures was different for each sample which was due to different amount of carbon coating on MoS$_2$. At high temperature, samples having higher amount of carbon gave less residue. From Figure 3.9, it can be seen that the most significant weight loss happened in sample synthesized using 2.5 g of glucose.
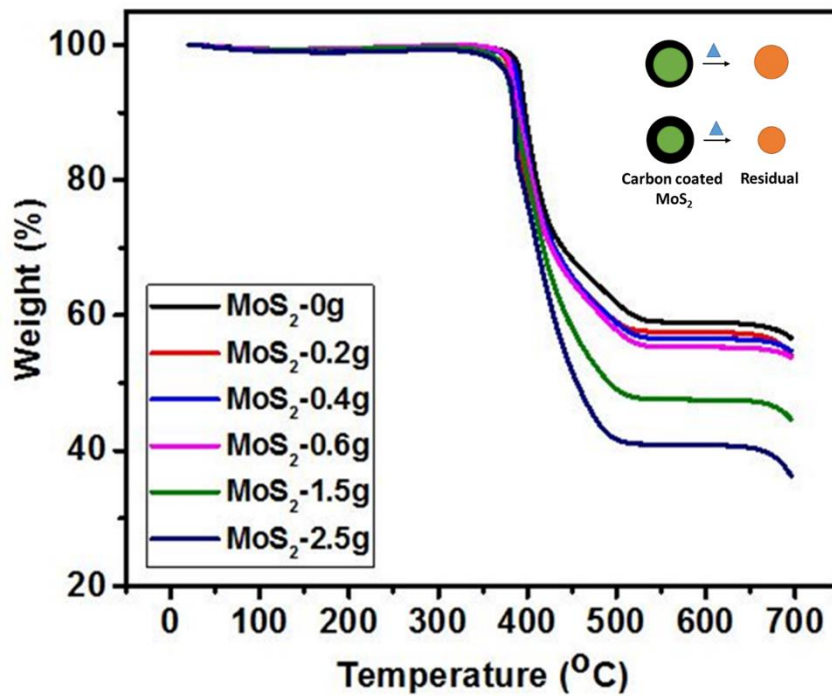
Figure 3.9: TGA analysis of various carbon coated MoS$_2$

Table 3.2: The carbon ratio of the sample with glucose after carbonized procedure

Glucose added (g)	Carbon ratio (%) 1st	Carbon ratio (%) 2nd	Average ratio (%)
0	37.72	36.60	37.16
0.2	39.32	37.94	38.63
0.4	39.57	41.59	40.58
0.6	42.51	41.81	42.16
1.5	54.07	49.89	51.98
2.5	57.16	55.72	56.44

3.6 Hydrogen evolution reaction (HER)

Linear scan voltammetry was performed on all the samples in potential range of 0 V to -0.47 V (vs RHE) at 0.005 V/s of scan rate. As seen in the LSV curve, pure molybdenum disulfide showed poor catalytic activity for splitting water to generate hydrogen whereas, carbon coated core-shelled molybdenum disulfide showed improved catalytic performance (Figure 3.10). It was observed that amount of carbon coating on MoS_2 had a significant effect on catalytic properties for HER applications. Especially, the sample with 0.2 g of glucose used during synthesis of MoS_2 showed the highest catalytic activity which was reflected by the deepest value of HER polarization curve in LSV (more than 16 mA /cm^2). Compared to previous results in Table 3.3, C@MoS_2 showed a very promising behavior for HER applications. The improved performance could be due to high surface area, conductivity and ease of electron transfer during the HER process.
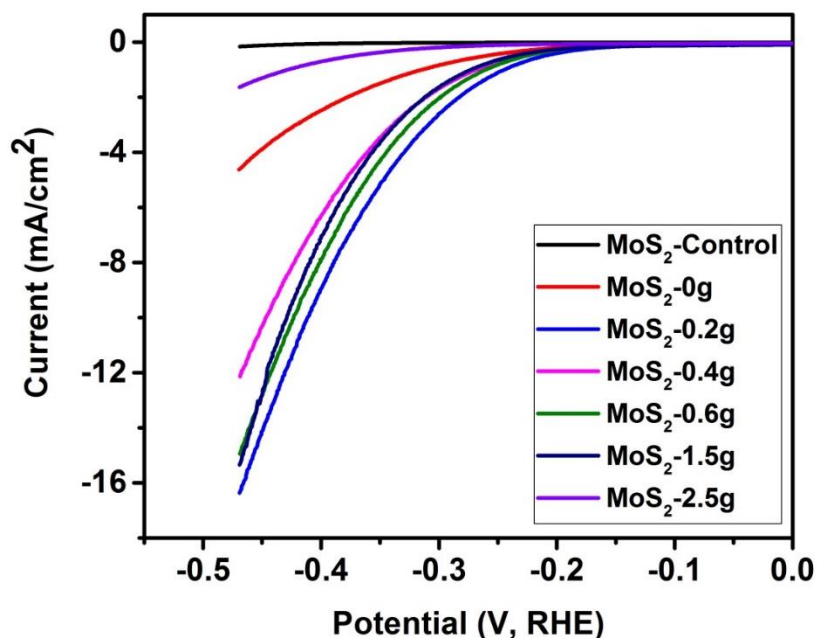
Figure 3.10: HER results of different samples

Table 3.3: Previous similar developments of transition metallic sulfide for HER[40, 41, 42]

Material	Current density
Cu_2MoS_4	12 mA/cm^2
Fe_xS_y mixture	7.2 mA/cm^2
Co_9S_8	14 mA/cm^{-2}

Additionally, Tafel slope was determined using LSV data of each sample. Fig 3.11 shows the Tafel slope of all the samples. The lowest Tafel slope of 133 mV was observed for MoS_2 synthesized using 0.2 g of glucose. The lower Tafel slope suggest better kinetic process during the HER process. Table 3.4 compares the Tafel slope of some other transition metallic sulfide

based compounds. As evident, carbon coated MoS$_2$ core-shell microsphere showed lowest Tafel

slope suggesting improved kinetics which could be due to improve conductivity.
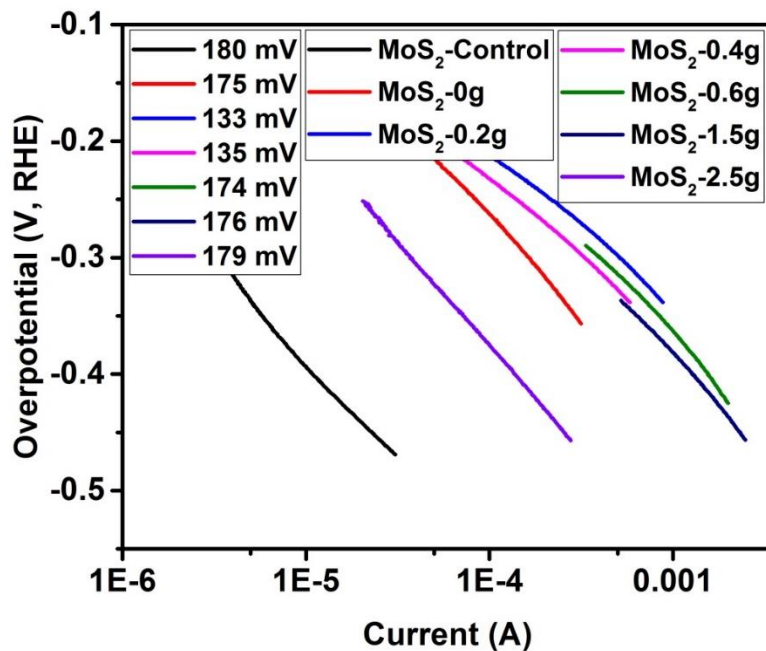
Figure 3.11: Tafel slope of various samples

Table 3.4: Tafel slope for hydrogen of platinum and common transition metallic sulfide catalysts

in splitting water [43]

Materials of the electrode	Tafel slope for hydrogen (V)
Platinum (Pt)	-0.07
FeS$_2$	-0.217
NiS$_2$	-0.23
(Fe$_{0.07}$Ni$_{0.93}$)S$_2$	-0.196
(Fe$_{0.48}$Co$_{0.52}$)S$_2$	-0.143
(Co$_{0.59}$Ni$_{0.41}$)S$_2$	-0.17

However, it was also observed that higher amount of carbon coating decreased the catalytic activity of MoS_2. These results were quite surprising as the prediction that the conducting carbon coating would constantly improve the catalytic activity of the MoS_2. An assumption was that overdose of glucose during synthesis of MoS_2 generate thick layer of carbon on MoS_2 which blocked the catalytic sites of MoS_2. Hence, optimum carbon layer thickness was required for MoS_2 to act as good catalyst for HER application.

3.7 Electrochemical impedance spectroscopy (EIS)

Electrochemical impedance spectroscopy was used to further study the electrochemical properties of the synthesized samples. Figure 3.12 shows variation of real and imaginary impedance as a function of frequency for all the samples. It was seen that MoS_2 synthesized using 0.2 g of glucose showed the lowest charge transfer resistance (smallest diameter) compared with other samples, indicating better electron transfer during hydrogen evolution study.
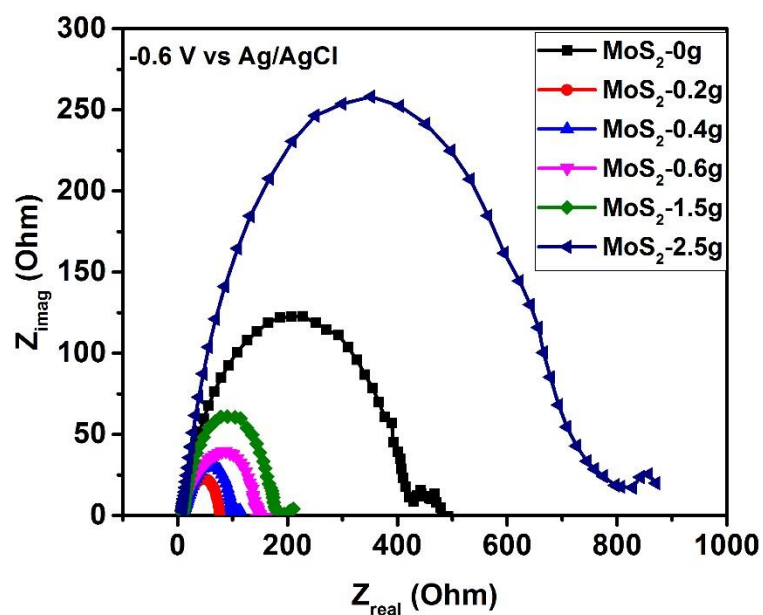
Figure 3.12: Z_{real} versus $Z_{imaginary}$ plots of all the MoS$_2$ samples synthesized using various amount

of glucose.

Figure 3.13 shows the variation of total impedance as a function of frequency for all the samples at room temperature. As seen in the figure, carbon coated MoS$_2$ synthesized using 0.2 g of glucose showed the lowest impedance, which was in good agreement with LSV and Z_{real} versus $Z_{imaginary}$ studies. The phenomenon of enhanced conductivity by carbon-coating could be attributed to the good conductivity of carbonized nanowall from glucose [44].
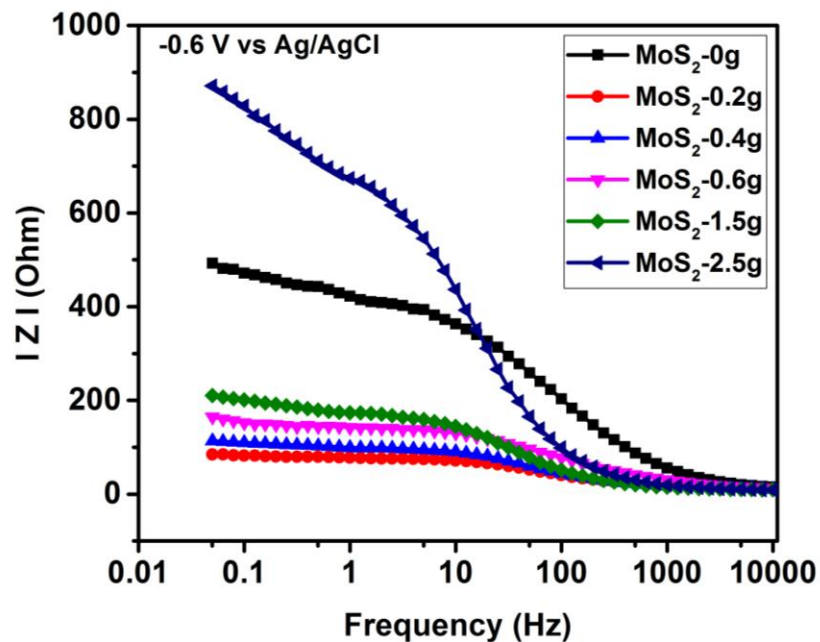
Figure 3.13: Impedance vs AC frequency for EIS test of the carbon coating C@MoS$_2$ core-shell

microspheres with different glucose content

3.8 Cyclic voltammetry (CV) for HER

Cyclic voltammetry was used to estimate active electrochemical surface area of the carbon coated MoS$_2$ samples. Figure 3.14 shows the CV curves of all the samples in non-Faradic region. As seen in the CV curves, the highest electrochemical surface area was observed for the MoS$_2$ sample synthesized using 0.2 g of glucose which showed the best catalytic activity for HER application.
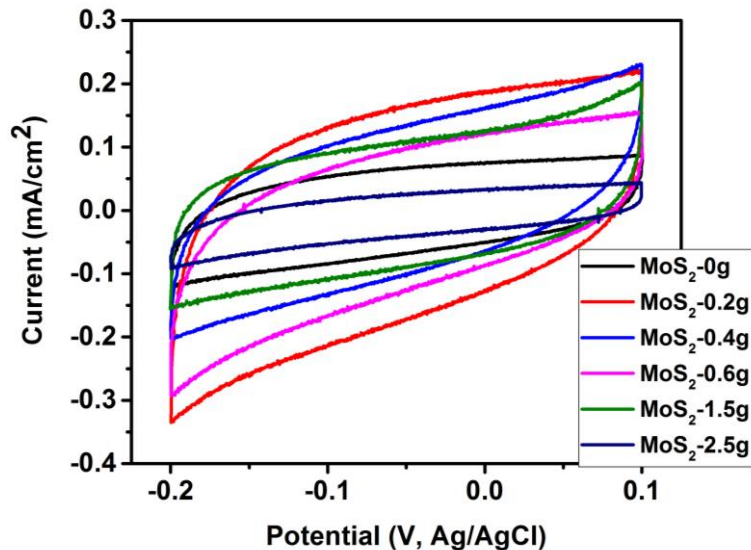
Figure 3.14: CV test for all the samples in non-Faradic region.

3.9 Cyclic voltammetry (CV) for supercapacitor application

The performance of carbon coated MoS_2 for energy storage application was tested using CV and GCD methods. Figure 3.15 shows the CV curves of all the samples in 3M KOH electrolyte at scan rate of 50 mV/s. Several redox peaks were observed in the CV curves indicating prominent pseudocapacitive behavior of the MoS_2 based electrodes. MoS_2 synthesized using 0.2 g of glucose exhibited the largest area under the CV curves, suggesting the maximum charge storage capacity. Gravimetric capacitance of each sample was calculated using equation 2.1 at different scan rates and illustrated in the Fig 3.16. The gravimetric capacitance decreased with increase in scan rate for all the samples which could be due to the limited time for transition of electrolyte ions and electron transfer process. Figure 3.17 shows the CV curves of MS-2 sample at various scan rates. As seen the shape and nature of the CV curves were similar even at higher scan rates, suggesting high rate capability of carbon coated MoS_2 samples. The highest capacitance of 345 F/g was observed for uncoated MoS_2 sample. However, the charge storage capacity of uncoated MoS_2 sample decayed faster than carbon coated MoS_2 samples. At higher

scan rates, MoS$_2$ synthesized using 0.2 g of glucose exhibited the higher charge storage capacity and better capacitance retention than uncoated and other carbon coated MoS$_2$ samples.
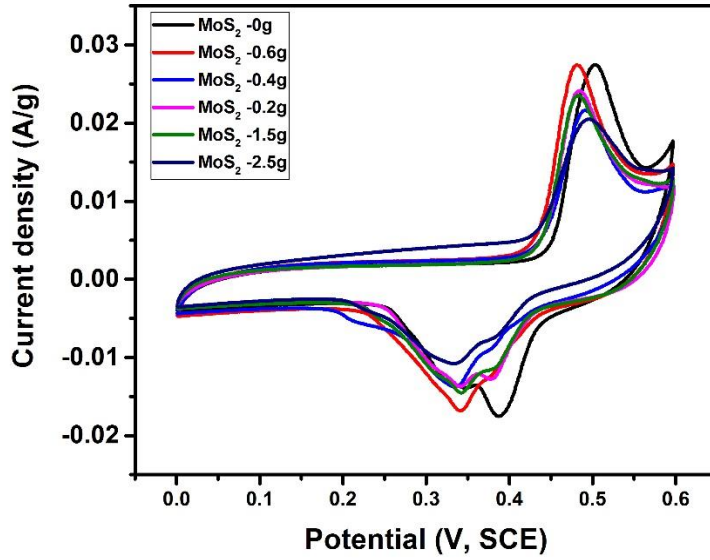
Figure 3.15: CV curves of uncoated and carbon coated MoS$_2$ samples at a scan rate of 50 mV/s
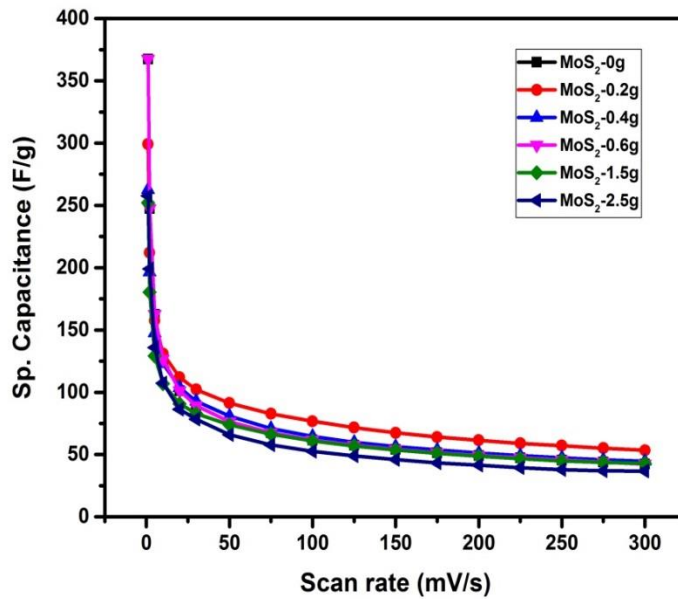
Figure 3.16: Variation of specific capacitance as a function of scan rates for all the samples
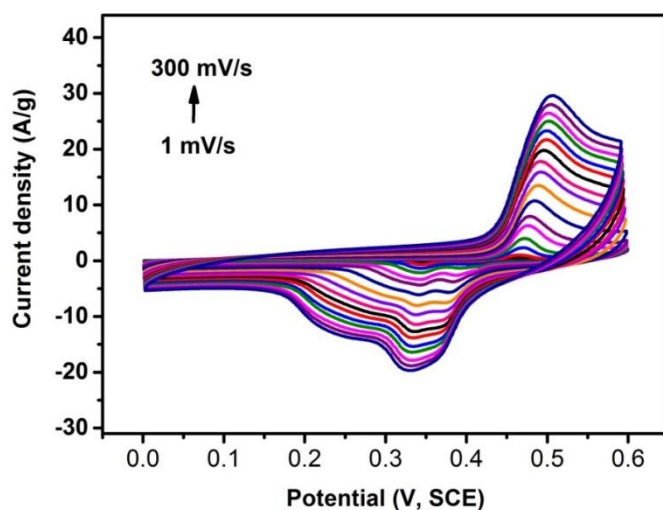
Figure 3.17: CV curves of MS-2 sample at various scan rates

3.10 Galvanostatic charge-discharge method (CD) for supercapacitor application

Electrochemical properties of MoS_2 based electrodes were further studied using galvanostatic charge-discharge method in 3M KOH electrolyte. The discharge characteristics measured at 0.25 A/g for uncoated and carbon coated MoS_2 are shown in Figure 3.18. Pseudocapacitive behavior of MoS_2 was further established by the non-linearity of the discharge profiles. As seen in the discharge curves, MoS_2 synthesized using 0.2 g of glucose showed the maximum discharge time, indicating higher charge storage capacity. Specific capacitance as a function of discharge current for all the samples was calculated using equation 2.2 and displayed in Figure 3.19. As evident from the graph, MoS_2 synthesized using 0.2 g of glucose exhibited the highest charge storage capacity across the total current density range, confirming the appropriate amount of carbon coating was required to maximize the electrochemical charge storage capacity. Specific capacitance of all the samples decreased with increasing current

36

density, suggesting an insufficient time for the Faradic reaction at electrode-electrolyte interface.
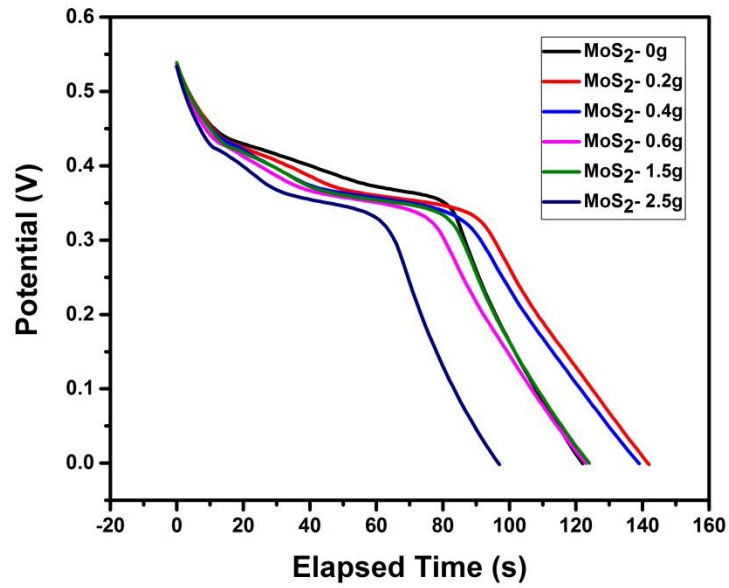
Figure 3.18: Galvanostatic charge-discharge profiles of various MoS$_2$ samples at a current density of 0.25 A/g
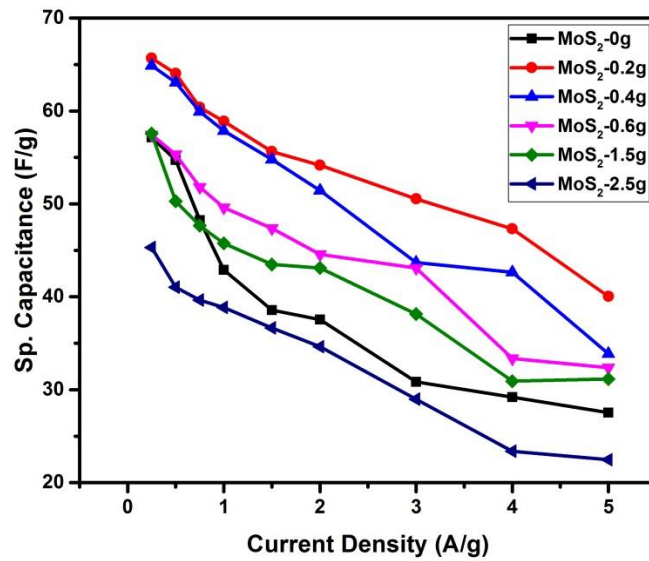
Figure 3.19: Effect of current density on specific capacitance of various MoS$_2$ samples

CHAPTER IV

CONCLUSION

A facile hydrothermal reaction was used for the synthesis of carbon coated MoS_2 using melamine, resorcinol and formaldehyde as the carbon precursors, sodium molybdate (Na_2MoO_4) as the molybdenum precursor and thiourea (NH_2CSNH_2) as the sulfur source. The synthesized MoS_2 samples were structurally and electrochemically characterized for their applications in hydrogen evolution reaction and energy storage devices.

It was observed that appropriate amount of glucose for carbon coating was crucial to achieve high catalytic activity and energy storage capacity. The MoS_2 synthesized using 0.2 g of glucose showed the best catalytic performance among the studied samples. CV studies in non-Faradic region confirmed that MoS_2 synthesized using 0.2 g of glucose had the highest electrochemical active surface area. Electrochemical impedance spectroscopy studies also confirmed the superior properties of MoS_2 synthesized using 0.2 g of glucose. In addition to superior catalytic property, these samples showed high charge storage capacity of about 300 F/g. Further the results of galvanostatic charge-discharge studies supported the results of CV measurements. Based on the results, carbon coated MoS_2 could be very promising material for energy generation and storage applications.

REFERENCES

1. Andújar, J. M., & Segura, F. (2009). Fuel cells: History and updating. A walk along two centuries. *Renewable and sustainable energy reviews, 13*, 2309-2322.

2. Ehsani, Mehrdad, Yimin Gao, and Ali Emadi. Modern electric, hybrid electric, and fuel cell vehicles: fundamentals, theory, and design. *CRC press*, 2009.

3. Song, Shuqin, and Panagiotis Tsiakaras. Recent progress in direct ethanol proton exchange membrane fuel cells (DE-PEMFCs) (2006). Applied Catalysis B: Environmental 63: 187-193.

4. Kordesch, K., Hacker, V., Reichmann, K., Cifrain, M., Hejze, T., & Aronsson, R. R. (2008). The safe and economic revival of alkaline hydrogen/air fuel cells with circulating electrolytes, recommended for vehicles using battery hybrid systems and H_2 from ammonia crackers. *ECS Transactions*, *11*, 167-185.

5. Nice, Karim, and Jonathan Strickland. How Fuel Cells Work: Polymer Exchange Membrane Fuel Cells. *How Stuff Works, accessed 4* (2011). http://auto.howstuffworks.com/fuel-efficiency/alternative-fuels/fuel-cell.htm

6. Yasuda, K., Taniguchi, A., Akita, T., Ioroi, T., & Siroma, Z. (2006). Platinum dissolution and deposition in the polymer electrolyte membrane of a PEM fuel cell as studied by potential cycling. *Physical Chemistry Chemical Physics*, *8*, 746-752.

7. Amphlett, J. C., Baumert, R. M., Mann, R. F., Peppley, B. a, Roberge, P. R., & Rodrigues, A. (1997). The effect of Carbon Monoxide contamination on Anode Efficiency in PEM Fuel Cells. Energy Conversion Engineering Conference, 1997*. IECEC-97.,* Proceedings of the 32nd Intersociety, 1477–1482.

8. Chen Chen, Yijin Kang, Ziyang Huo, Zhongwei Zhu, Wenyu Huang, Huolin L. Xin, Joshua D. Snyder, Dongguo Li, Jeffrey A. Herron, Manos Mavrikakis, Miaofang Chi, Karren L. More, Yadong Li, Nenad M. Markovic, Gabor A. Somorjai, P. Y. and V. R. S. (2014). Highly

Crystalline Multimetallic Nanoframes with Three-Dimensiona/Electrocatalytic Surfaces. *Science, 343*, 1339–1343.

9. Yuan, H., Li, J., Yuan, C., & He, Z. (2014). Facile Synthesis of MoS_2@CNT as an Effective Catalyst for Hydrogen Production in Microbial Electrolysis Cells. *ChemElectroChem, 1*, 1828–1833.

10. Saminathan, K., Kamavaram, V., Veedu, V., & Kannan, A. M. (2009). Preparation and evaluation of electrodeposited platinum nanoparticles on in situ carbon nanotubes grown carbon paper for proton exchange membrane fuel cells. *International Journal of Hydrogen Energy, 34*, 3838–3844.

11. Chen, S., Zhu, J., Wu, X., Han, Q., & Wang, X. (2010). Graphene oxide− MnO_2 nanocomposites for supercapacitors. *ACS nano, 4*, 2822-2830.

12. Xia, X., Zhu, C., Luo, J., Zeng, Z., Guan, C., Ng, C.F., Zhang, H. and Fan, H.J. (2014). Synthesis of Free‐Standing Metal Sulfide Nanoarrays via Anion Exchange Reaction and Their Electrochemical Energy Storage Application. *small*, *10*, 766-773.

13. Ma, G., Peng, H., Mu, J., Huang, H., Zhou, X., & Lei, Z. (2013). In situ intercalative polymerization of pyrrole in graphene analogue of MoS_2 as advanced electrode material in supercapacitor. *Journal of Power Sources, 229*, 72-78.

14. Barbieri, O., Hahn, M., Herzog, A., & Kötz, R. (2005). Capacitance limits of high surface area activated carbons for double layer capacitors. *Carbon,43*, 1303-1310.

15. Wang, D.Y., Gong, M., Chou, H.L., Pan, C.J., Chen, H.A., Wu, Y., Lin, M.C., Guan, M., Yang, J., Chen, C.W. and Wang, Y.L. (2015). Highly active and stable hybrid catalyst of cobalt-doped FeS_2 nanosheets-carbon nanotubes for hydrogen evolution reaction. *Journal of the American Chemical Society, 137*, 1587–1592.

16. Universiti Sains Malaysia. "New method for continuous production of carbon nanotubes." *ScienceDaily*, 12 April 2012.
https://www.sciencedaily.com/releases/2012/04/120412105109.htm

17. Sun, F., Wei, Y., Chen, J., Long, D., Ling, L., Li, Y., & Shi, J. (2015). Melamine-assisted one-pot synthesis of hierarchical nitrogen-doped carbon@ MoS_2 nanowalled core–shell microspheres and their enhanced Li-storage performances. *Nanoscale*, *7*, 13043-13050.

18. Millington, B., Du, S., & Pollet, B. G. (2011). The effect of materials on proton exchange membrane fuel cell electrode performance. *Journal of Power Sources, 196*, 9013-9017.

19. Kim, Yun-Sung; Lim, Jun-Heok; Chun, Hai-Soo (2006). "Creep mechanism of porous MCFC Ni anodes strengthened by Ni_3Al". *AIChE Journal. 52*: 359–365.

20. Wang, H., Feng, H., & Li, J. (2014). Graphene and graphene-like layered transition metal dichalcogenides in energy conversion and storage. *Small, 10*, 2165–2181.

21. Jing, Y., Zhou, Z., Cabrera, C. R., & Chen, Z. (2014). Graphene, inorganic graphene analogs and their composites for lithium ion batteries. *Journal of Materials Chemistry A, 2*, 12104-12122.

22. Fang, X., Yu, X., Liao, S., Shi, Y., Hu, Y.S., Wang, Z., Stucky, G.D. and Chen, L. (2012). Lithium storage performance in ordered mesoporous MoS_2 electrode material. *Microporous and Mesoporous Materials, 151*, 418-423.

23. Shi, Y., Wang, Y., Wong, J.I., Tan, A.Y.S., Hsu, C.L., Li, L.J., Lu, Y.C. and Yang, H.Y. (2013). Self-assembly of hierarchical MoSx/CNT nanocomposites (2< x< 3): towards high performance anode materials for lithium ion batteries. *Scientific reports*, *3*, 2169.

24. Yu, H., Zhu, C., Zhang, K., Chen, Y., Li, C., Gao, P., Yang, P. and Ouyang, Q. (2014). Three-dimensional hierarchical MoS_2 nanoflake array/carbon cloth as high-performance flexible lithium-ion battery anodes. *Journal of Materials Chemistry A*, *2*, 4551-4557.

25. X Xiao, J., Choi, D., Cosimbescu, L., Koech, P., Liu, J., & Lemmon, J. P. (2010). Exfoliated MoS_2 nanocomposite as an anode material for lithium ion batteries. *Chemistry of Materials*, *22*, 4522-4524.

26. Du, G, Guo, Z., Wang, S., Zeng, R., Chen, Z., & Liu, H. (2010). Superior stability and high capacity of restacked molybdenum disulfide as anode material for lithium ion batteries. *Chemical communications*, *46,* 1106-1108.

27. Chang, K., Chen, W., Ma, L., Li, H., Li, H., Huang, F., Xu, Z., Zhang, Q. and Lee, J.Y. (2011). Graphene-like MoS$_2$/amorphous carbon composites with high capacity and excellent stability as anode materials for lithium ion batteries. *Journal of Materials Chemistry*, *21*(17), 6251-6257.

28. Zhang, C., Wang, Z., Guo, Z., & Lou, X. W. (2012). Synthesis of MoS$_2$–C one-dimensional nanostructures with improved lithium storage properties. *ACS applied materials & interfaces*, *4*, 3765-3768.

29. Bindumadhavan, K., Srivastava, S. K., & Mahanty, S. (2013). MoS$_2$ –MWCNT hybrids as a superior anode in lithium-ion batteries. *Chemical Communications*, *49*, 1823-1825.

30. Ding, S., Chen, J. S., & Lou, X. W. D. (2011). Glucose‑Assisted Growth of MoS$_2$ Nanosheets on CNT Backbone for Improved Lithium Storage Properties. *Chemistry–A European Journal*, *17*, 13142-13145.

31. Zhou, X., Wan, L. J., & Guo, Y. G. (2012). Facile synthesis of MoS$_2$@ CMK-3 nanocomposite as an improved anode material for lithium-ion batteries. *Nanoscale*, *4*, 5868-5871.

32. Das, S. K., Mallavajula, R., Jayaprakash, N., & Archer, L. A. (2012). Self-assembled MoS$_2$ – carbon nanostructures: influence of nanostructuring and carbon on lithium battery performance. *Journal of Materials Chemistry*, *22*, 12988-12992.

33. Chang, K., & Chen, W. (2011). Single-layer MoS$_2$/graphene dispersed in amorphous carbon: towards high electrochemical performances in rechargeable lithium ion batteries. *Journal of Materials Chemistry*, *21*, 17175-17184.

34. Chang, K., & Chen, W. (2011). In situ synthesis of MoS$_2$/graphene nanosheet composites with extraordinarily high electrochemical performance for lithium ion batteries. *Chemical Communications*, *47*, 4252-4254.

35. Sen, U. K., & Mitra, S. (2013). High-rate and high-energy-density lithium-ion battery anode containing 2D MoS$_2$ nanowall and cellulose binder. *ACS applied materials & interfaces*, *5*, 1240-1247.

36. Hwang, H., Kim, H., & Cho, J. (2011). MoS$_2$ nanoplates consisting of disordered graphene-like layers for high rate lithium battery anode materials. *Nano letters*, *11*, 4826-4830.

37. Bard AJ, Faulkner LR, Leddy J, Zoski CG. *Electrochemical methods: fundamentals and applications*. Vol. 2. New York: Wiley, 1980.

38. Faber, M. S., Lukowski, M. a, Ding, Q., Kaiser, N. S., & Jin, S. (2014). Earth-Abundant Metal Pyrites (FeS_2 , CoS_2 , NiS_2 , and Their Alloys) for Highly Efficient Hydrogen Evolution and Polysulfide Reduction Electrocatalysis. *The Journal of Physical Chemistry C, 118*, 21347–21356.

39. Wu H, Yang R, Song B, Han Q, Li J, Zhang Y, Fang Y, Tenne R, Wang C. (2011). Biocompatible inorganic fullerene-like molybdenum disulfide nanoparticles produced by pulsed laser ablation in water. *ACS nano*, *5*, 1276-1281.

40. Zheng, X., Xu, J., Yan, K., Wang, H., Wang, Z., & Yang, S. (2014). Space-confined growth of MoS_2 nanosheets within graphite: the layered hybrid of MoS_2 and graphene as an active catalyst for hydrogen evolution reaction. *Chemistry of Materials*, *26*, 2344-2353.

41. Zhu, H., Lyu, F., Du, M., Zhang, M., Wang, Q., Yao, J., & Guo, B. (2014). Design of two-dimensional, ultrathin MoS_2 nanoplates fabricated within one-dimensional carbon nanofibers with thermosensitive morphology: high-performance electrocatalysts for the hydrogen evolution reaction. *ACS applied materials & interfaces*, *6*, 22126-22137.

42. Lee, C., Yan, H., Brus, L. E., Heinz, T. F., Hone, J., & Ryu, S. (2010). Anomalous lattice vibrations of single-and few-layer MoS_2. *ACS nano*, *4*, 2695-2700.

43. Feng, L.L., Li, G.D., Liu, Y., Wu, Y., Chen, H., Wang, Y., Zou, Y.C., Wang, D. and Zou, X. (2015). Carbon-armored Co_9S_8 nanoparticles as all-pH efficient and durable H_2-evolving electrocatalysts. *ACS applied materials & interfaces*, *7*, 980-988.

44. Tran, P.D., Nguyen, M., Pramana, S.S., Bhattacharjee, A., Chiam, S.Y., Fize, J., Field, M.J., Artero, V., Wong, L.H., Loo, J. and Barber, J. (2012). Copper molybdenum sulfide: a new efficient electrocatalyst for hydrogen production from water. *Energy & Environmental Science*, *5*, 8912-8916.